ECONOMIT JOURNAL
SCIENTIFIC JOURNAL OF ACCOUNTANCY, MANAGEMENT, AND FINANCE

# Future Compound Heat-Flash Drought Events Amplify Socioeconomic Exposure and Human Displacement Risks across East Africa

**Belay Sitotaw Goshu[1], Muhammad Ridwan[2]**
[1]Department of Physics, Dire Dawa University, Dire Dawa, Ethiopia
[2]Universitas Islam Negeri Sumatera Utara, Indonesia
Email: belaysitotaw@gmail.com, bukharyahmed@gmail.com

***Abstract:***
*East Africa faces an escalating climate crisis driven by the amplification of compound heat-flash drought (CHFD) events. This study quantifies future CHFD dynamics, socioeconomic exposure, agricultural impacts, and human displacement risks across East Africa under moderate (SSP2-4.5) and high-emissions (SSP5-8.5) scenarios. Using a weighted multi-model ensemble from CMIP6 projections, we analyze historical (1981–2010) and future (2021–2100) periods, integrating population density data, agricultural statistics, and displacement modeling frameworks. Under SSP5-8.5, moderate CHFD frequency is projected to double, while severe events increase by 60% by 2100. Population exposure increases by up to 60% in southern Tanzania and 40–55% in northeastern Kenya, southern Somalia, and eastern Ethiopia. Compound drought-heatwave exposure is linked to 27% (±4.2%) reductions in harvested area and 35% (±5.1%) reductions in crop production, with maize and sorghum most severely affected ($\beta = -0.47$ to $-0.53$, $p < 0.01$). Rain-fed systems suffer losses exceeding 30%, while irrigated systems demonstrate resilience with losses below 10%. Climate change, accounting for 57.4–71.2% of exposure changes, is the primary driver, with population growth contributing 18.5–26.8%. Climate change could force 6.9–10.1 million people in East Africa to move internally by 2050. These findings demand urgent emission reductions, as mitigation is the most effective strategy for reducing future risks. Adaptation priorities include climate-resilient crops, irrigation expansion, improved flash drought early warning systems, social protection for vulnerable populations, and migration governance frameworks. Region-specific strategies are essential given East Africa's heterogeneous climate responses.*
***Keywords:***
*Compound extremes; Flash drought; Population exposure; Human displacement; East Africa*

## I. Introduction

### 1.1 Background and Rationale

East Africa stands at the frontline of global climate change impacts. The region encompassing countries such as Kenya, Tanzania, Ethiopia, Somalia, Uganda, and South Sudan, exhibits profound vulnerability to climate extremes, driven by a confluence of factors including large and rapidly growing populations, low adaptive capacity, heavy dependence on rain-fed agriculture, and recurring socio-political fragility. This vulnerability is compounded by the region's climatic heterogeneity, which ranges from the arid and semi-arid lowlands to the humid highlands, creating a mosaic of distinct but interconnected climate risks.

In recent years, a paradigm shift has occurred in climate risk science. Individual extreme events; droughts, heatwaves, floods are no longer the sole focus of concern. Instead, compound extremes, where multiple hazards co-occur or cascade within the same location and time frame, have emerged as a more dangerous class of climate risk. Muheki et al. (2024)


*DOI: https://doi.org/10.5281/zenodo.21769574*

demonstrated that co-occurring extreme events will become "the norm rather than the exception" in East Africa, even under low-end warming scenarios, with the strongest increases projected for joint heatwaves and wildfires (+940% by the end of the century under RCP6.0), followed by river floods and heatwaves (+900%) and river floods and wildfires (+250%). This finding underscores a critical reality: the impacts of multiple concurrent extremes are not merely additive but synergistic, producing consequences far greater than the sum of their parts.

Within the broader category of compound extremes, compound drought-heatwave events (CDHEs), also referred to as compound hot-dry extremes (CHDEs) have attracted particular scientific attention. These events occur when drought conditions (precipitation deficits and soil moisture depletion) coincide with elevated temperatures, creating mutually reinforcing thermal and hydrological stresses. The mechanisms driving CDHEs are well-established: high temperatures increase evaporative demand, accelerating soil moisture loss, which in turn reduces evaporative cooling and further elevates surface temperatures, a positive feedback loop that amplifies both hazards.

A particularly insidious manifestation of this phenomenon is the flash drought, a rapidly intensifying drought that develops over weeks rather than seasons, typically driven by anomalously high temperatures, winds, and radiation that lead to abnormally high evapotranspiration rates. Unlike conventional droughts, which are primarily driven by precipitation deficits and unfold over seasonal to interannual timescales, flash droughts challenge existing forecasting systems because they evolve faster than the temporal resolution of most drought indicators. Li et al. (2026) documented that anthropogenic warming and vegetation greening have driven a recent surge in flash droughts globally, exposing approximately 650 million people to threat and substantially reducing gross primary productivity. The distinction between flash and conventional droughts is not merely academic; it has profound implications for early warning, preparedness, and response, as flash droughts can devastate agricultural systems with little to no advance notice.

Historical evidence from the Horn of Africa underscores the escalating nature of this threat. Alasow et al. (2024) examined the spatiotemporal patterns of CDHW periods across three periods (1951–1980, 1971–2000, and 1991–2020) and found a substantial increase in the duration of CDHW events in recent years, with durations reaching up to 25 days. The average duration of heatwaves increased from 7 days before 1993 to 18 days by 2011, culminating in a record-breaking 43-day heatwave in 2019. Most areas experienced a significant increase in heatwave duration by more than 12 days from the early period to the most recent period, with Ethiopia and Kenya experiencing substantial increases of more than 18 days during the most recent period, and some duration exceeding 25 days in recent decades.

The agricultural implications of these trends are severe. Abdelrahim and Jin (2026) analyzed CDHE spatiotemporal patterns and impacts across Eritrea, Ethiopia, Somalia, and Djibouti from 2000 to 2022, documenting a 140% cumulative expansion of CDHE-impacted areas, with more than 45% of the Horn of Africa impacted annually by 2022. Regression models linked CDHE exposure to 27% (± 4.2%) and 35% (± 5.1%) reductions in harvested area and crop production, respectively, with maize and sorghum; key staples most severely affected ($\beta = -0.47$ to $-0.53$, $p < 0.01$). Southern Somalia and eastern Ethiopia rain-fed systems suffered more than 30% losses, driven by soil degradation, water stress, and heat stress at sensitive growth stages. In contrast, Ethiopia's irrigated highlands were more resilient (< 10% losses) due to drought-tolerant crops and water management, highlighting the protective role of adaptive agricultural practices.

### 1.2 Research Gap and Problem Statement

Despite growing recognition of the threats posed by compound climate extremes, significant knowledge gaps persist regarding their dynamics, impacts, and implications specifically for East Africa under future warming scenarios.

First, while global studies have documented the increasing frequency of compound drought-heatwave events, region-specific analyses for East Africa remain limited. Ayugi et al. (2024) made a significant contribution by analyzing observed and future CHDEs over East Africa using a weighted multi-model ensemble from CMIP6 projections, finding that under SSP5-8.5, the frequency of moderate CHDE will double, and severe CHDE will increase by 60% relative to baseline, with southern Tanzania and northeastern Kenya identified as the most affected regions. However, comprehensive assessments with robust signal-to-noise analyses across multiple models and scenarios are still needed to establish confidence in these projections and to understand the full range of uncertainty.

Second, the translation of physical climate hazards into socioeconomic exposure and human displacement outcomes remains insufficiently quantified. While Ayugi et al. (2024) projected that population exposure to CHDEs could increase by up to 60% in parts of southern Tanzania under future scenarios; the mechanisms through which compound events drive agricultural losses, livelihood disruption, and ultimately migration are not well understood. The cascading effects from agricultural collapse to displacement have not been systematically modeled for East Africa, leaving a critical gap in understanding the full impact pathway from climate hazard to human outcome.

Third, there is a critical need for spatially explicit, policy-relevant projections that can inform regional adaptation planning and disaster risk reduction. The heterogeneous response of East Africa's agro-climate regime to climate changes demands differentiated, location-specific policy responses. Current research often treats East Africa as a monolithic region, obscuring the differential vulnerabilities and adaptation needs across its diverse landscapes and communities (Demissie et al., 2025).

Fourth, the displacement implications of compound climate extremes have received fragmented attention. The World Bank's Groundswell report projects that over 216 million people could move within their countries by 2050 across six regions (World Bank, 2021). For East Africa specifically, estimates indicate that between 6.9 and 10.1 million people may be forced to relocate due to climate-related factors by 2050, with broader estimates suggesting that as many as 38.5 million people in East Africa could be forcibly displaced. However, the specific contribution of compound heat-flash drought events to these displacement projections has not been disaggregated, leaving a critical gap in understanding the drivers of climate mobility in the region.

Collectively, these gaps underscore the urgent need for an integrated assessment that links future compound heat-flash drought dynamics to socioeconomic exposure, agricultural impacts, and human displacement risks across East Africa.

# II. Review of Literature

## 2.1 Compound Climate Extremes: Definitions and Global Trends

The concept of compound climate extremes has emerged as a paradigm-shifting framework in climate risk science. First introduced by the Intergovernmental Panel on Climate Change in 2012, compound weather events refer to combinations of multiple climate drivers and hazards that interact to create amplified societal and environmental risks (Castet, 2024). Unlike isolated extreme events, these overlapping phenomena involve a complex interplay of factors, leading to impacts that are far greater than the sum of their parts.

Compound extremes can be classified into three distinct typologies. Temporally compounding events involve successive hazards occurring in the same geographical area, for example, heatwaves followed by droughts, which significantly elevate wildfire risks. Research shows that wildfires are 62% more likely during such compounded conditions compared to droughts alone, and 26% more likely than during isolated heat events. Multivariate compounding events involve the simultaneous occurrence of multiple hazards within the same region, such as the co-occurrence of drought and heat during critical crop flowering periods. This combination has been shown to drastically reduce agricultural yields, with a 70% chance of below-average production during such events, compared to only a 50% probability during isolated droughts or heat events. Spatially compounding events occur when a single hazard affects multiple, connected regions simultaneously. As defined more broadly, compound extremes are the simultaneous or sequential occurrence of multiple environmental stressors over the same geographical region that collectively represent extreme hazardous conditions (Ashfaq et al., 2021).

The global escalation of compound drought–heatwaves (CDHWs) has been well documented. Fan et al. (2024) introduced the concept of soil compound drought–heatwaves (SCDHWs) to provide a more objective assessment of concurrent water and heat stresses in global soils, revealing that the intensity and growth rate of global SCDHW events are substantially greater and accelerate more quickly than previously estimated from a meteorological perspective. Their analysis demonstrated a global escalation in the frequency, duration, peak intensity, and severity of SCDHWs, as well as an increase in affected land area, from 1980 to 2023, with trends particularly prominent since the early 2000s and projected to persist throughout this century. Approximately 57% of global land areas have been affected by these escalating compound events.

## 2.2 Flash Droughts: Characteristics and Drivers

Flash droughts represent a particularly insidious manifestation of rapid-onset drought that has emerged as a defining hydroclimatic extreme in a warming climate (2026). Characterized by their unusually rapid onset and intensification—typically developing within days to a few weeks, flash droughts challenge existing forecasting systems because they evolve faster than the temporal resolution of most drought indicators. The rapid development of these events often limits the effectiveness of early warnings and frequently results in widespread crop failures, water shortages, and terrestrial carbon loss.

The mechanisms driving flash droughts have undergone a fundamental shift in recent decades. Using an explainable artificial intelligence–based clustering framework with reanalysis products and Earth system models, Li et al. (2026) demonstrated that the major driving mechanisms of global flash droughts have shifted from precipitation dominance to a compound effect of temperature, transpiration, and precipitation. This transition drives a surge in flash droughts, with more rapidly developing, severe, and enduring soil droughts. Anthropogenic warming and vegetation greening are identified as the main drivers of the observed surge. The transition, which has emerged beyond natural climate variability since 2017 and is mainly detected in Eurasia, the Amazon, and Africa, exposes approximately 650 million people to threat and reduces gross primary productivity by 0.15 ± 0.1 petagrams of carbon per year.

The physical processes underlying flash drought intensification are increasingly well understood. Rising temperatures increase atmospheric evaporative demand, accelerating soil moisture loss through elevated evapotranspiration. The presence of extreme heat during flash droughts accelerates soil moisture drawdown, with the severity being 6.7–90.8% higher and the recovery duration 8.3–114.3% longer for compound heat-flash droughts compared with non-heat flash droughts. These findings indicate that the processes and interactions giving rise to extreme heat during flash droughts significantly lengthen and exacerbate drought impacts. Research has also shown that temperature is increasingly surpassing precipitation as the dominant driver of flash drought acceleration under climate warming. As one study notes, "flash droughts are rapid-onset droughts that develop within days to a week", yet they remain rarely studied through the lens of evapotranspiration, the dominant flux driving changes in terrestrial water storage during such events.

### 2.3 East Africa's Climate Vulnerability

East Africa's vulnerability to climate extremes is shaped by a complex hydroclimate and socioeconomic context that makes the region particularly susceptible to climate change-induced hydrological extremes (2024). The region exhibits strong spatial heterogeneity in both current climate conditions and future projections, with marked seasonal contrasts and varying intensities across different sub-regions (2026).

Demissie et al. (2025) provided a comprehensive assessment of current and projected changes in climate extremes and agro-climatic zones over East Africa, utilizing ensembles of seven global climate models selected from the sixth Coupled Model Intercomparison Project (CMIP6) under SSP245 and SSP585 socioeconomic pathways. Their findings reveal several critical trends. First, all heat stress indicators, including the frequency of hot spells and the duration and intensity of heatwaves are projected to increase in future climates. Second, the frequency and intensity of heavy precipitation events are projected to increase with increased greenhouse gas emissions. Third, drought stress indicators follow the precipitation pattern and are projected to decline over most of the domain.

Perhaps most significantly, Demissie et al. (2025) documented a heterogeneous response of the agro-climate regime to climate changes projected for eastern Africa. Some areas, particularly southern Tanzania—are experiencing alterations toward drier zones, while others, such as northern Somalia and South Sudan—are experiencing a shift toward wetter zones. This heterogeneity has critical implications for agriculture and local livestock production, as the increase in short-duration heavy precipitation events together with the enhanced pace of heat stress will create divergent challenges across the region.

The region's high dependence on rain-fed agriculture and pastoralism, combined with limited adaptive capacity and large population sizes, amplifies its vulnerability. As noted in the broader literature, Africa is particularly vulnerable to climate extremes due to its limited adaptive capacity and high exposure to climate extremes. The East Africa region is one of the vulnerable areas exposed to water-related disasters, both floods and droughts. With rising temperatures of up to 5.5°C projected in hotspots such as Somalia and Eritrea (2026), the region faces an escalating threat to its agricultural systems and food security.

### 2.4 Compound Hot-Dry Extremes (CHDE) in East Africa: State of Knowledge

The state of knowledge regarding compound hot-dry extremes in East Africa has advanced considerably in recent years, with multiple studies documenting both historical trends and future projections. Ayugi et al. (2024) conducted a comprehensive analysis of the frequency, magnitude, and severity of observed and future CHDEs over East Africa, computing CHDE events from observed precipitation and maximum temperature data of the Climatic Research Unit gridded Timeseries version five (CRU TS). Their findings indicate a substantial amplification of CHDEs under future warming scenarios.

Alasow et al. (2024) examined the historical spatiotemporal patterns of compound drought and heatwave (CDHW) periods in the Horn of Africa during three periods (1951–1980, 1971–2000, and 1991–2020) using the ERA5 reanalysis dataset. Their analysis revealed a substantial increase in the duration of CDHW events in recent years, with durations reaching up to 25 days, and heatwave duration increasing from an average of 7 days before 1993 to 18 days by 2011. This escalating trend underscores the growing threat posed by compound extremes in the region.

Abdelrahim and Jin (2026) provided critical evidence on the expansion of CDHE-impacted areas in the Horn of Africa. Their results show a 140% cumulative expansion of CDHE-impacted areas, with more than 45% of the Horn of Africa impacted annually by 2022. This represents a dramatic and rapid expansion of compound extreme conditions across the region. The study also documented the devastating agricultural consequences of these events, with regression models linking CDHE exposure to 27% (± 4.2%) and 35% (± 5.1%) reductions in harvested area and crop production, respectively.

The intensification of CDHWs in Africa is further confirmed by recent research on coupled land–atmosphere processes. Using ERA5 and NCEP-2 reanalysis datasets for 1980–2024, researchers identified a pronounced hotspot in equatorial Africa, where CDHW frequency has increased by 0.9 events season$^{-1}$ decade$^{-1}$, duration by 1.2 days season$^{-1}$ decade$^{-1}$, and magnitude by 0.4 °C season$^{-1}$ decade$^{-1}$. Change-point analysis revealed two distinct periods: a modest increase of 0.4 events season$^{-1}$ decade$^{-1}$ during 1980–2003, followed by rapid intensification of 1.1 events season$^{-1}$ decade$^{-1}$ during 2005–2024. This recent intensification is driven primarily by stronger land–atmosphere coupling, with higher potential evaporation due to elevated maximum temperatures and declining soil moisture from reduced precipitation. The study also found an increased contribution of large-scale climate models, including the Atlantic meridional oscillation, Indian Ocean Dipole, and Pacific Decadal Oscillation to recent CDHW intensification.

## III. Research Methods

### 3.1 Study Area

This study focuses on the East Africa region, encompassing the countries of Kenya, Tanzania, Uganda, Ethiopia, Somalia, South Sudan, and neighboring territories that form the broader Eastern African hydroclimatic domain. This region is characterized by considerable climatic heterogeneity, ranging from the arid and semi-arid lowlands of the Horn of Africa to the humid highlands of Ethiopia and the equatorial lake regions of Uganda and Kenya. The study area is further delineated to include sub-regional hotspots identified in prior research as particularly vulnerable to compound hot-dry extremes, including southern Tanzania, northeastern Kenya, and the rain-fed agricultural zones of southern Somalia and eastern Ethiopia (Ayugi et al., 2024; Abdelrahim & Jin, 2026). This spatial delineation enables a focused assessment of regions where the convergence of high hazard frequency, high population exposure, and high agricultural vulnerability creates compound risks.


**Figure 1.** Study area in East Africa highlighting core countries and sub-regional hotspots vulnerable to compound hot-dry extremes (Ayugi et al., 2024).

### 3.2 Climate Data

#### a. Observational Data

Historical observational data are derived from the Climatic Research Unit (CRU) gridded Time-Series dataset version 4.05 (CRU TS4.05). This dataset provides monthly gridded fields of precipitation and maximum temperature at a spatial resolution of 0.5° × 0.5° for the period 1901–2020. The CRU TS4.05 data are based on monthly observational data calculated from daily or sub-daily records provided by National Meteorological Services and other external agents, making it a widely used and reliable product for climate studies in data-sparse regions such as East Africa. For this study, the baseline period 1981–2010 is used to establish reference climatological thresholds for identifying compound heat-flash drought events, consistent with established practices in the literature (Ayugi et al., 2024; Alasow et al., 2024).

#### b. Future Climate Projections

Future climate projections are obtained from the Coupled Model Intercomparison Project Phase 6 (CMIP6) multi-model ensemble. CMIP6 represents the most recent generation of global climate models, with improved performance in simulating temperature and precipitation patterns compared to previous CMIP3 and CMIP5 generations. To ensure robustness, a subset of CMIP6 models is selected based on data completeness, diversity in spatial resolution and structural design, and proven performance in simulating temperature and precipitation patterns over East Africa. The selected models include BCC-CSM2-MR, EC-Earth3, GFDL-ESM4, INM-CM5-0, IPSL-CM6A-LR, and MPI-ESM1-2-HR, among others. Model ensembles are known to outperform individual models, as they better capture the range of climate variability and reduce uncertainty.

Projections are analyzed under two Shared Socioeconomic Pathway (SSP) scenarios:

1. SSP2-4.5: A moderate emissions scenario representing a middle-of-the-road pathway with intermediate challenges to mitigation and adaptation.
2. SSP5-8.5: A high-emissions scenario representing rapid economic growth with fossil-fuel-intensive development, leading to the highest radiative forcing.

Future climate data are analyzed across four time periods to capture both near-term and long-term changes shown in Table 1.

**Table 1.** The period and the lone temporal range and their purpose

| Time Period | Temporal Range | Purpose |
|---|---|---|
| Baseline | 1981–2010 | Reference climatology for threshold definition |
| Near-future | 2021–2050 | Assessment of near-term changes |
| Mid-future | 2041–2070 | Assessment of medium-term changes |
| Far-future | 2071–2100 | Assessment of long-term changes under continued warming |

### 3.3 Definition of Compound Heat-Flash Drought Events

The identification of compound heat-flash drought (CHFD) events follows a threshold-based approach widely adopted in the literature. Thresholds are set using relative percentile values, which are preferred over absolute thresholds as they account for regional climatic variability (Hao et al., 2022).

#### a. Heatwave Definition

A heatwave is defined as a period of at least three consecutive days during which the daily maximum temperature exceeds the 90th percentile of the baseline period (1981–2010) for that specific calendar day. This definition is consistent with established methodologies in compound extremes research. To account for seasonal variability, the 90th percentile is calculated using a 31-day running window centered on the day under evaluation.

#### b. Drought Definition

A drought event is identified when monthly precipitation falls below the 25th percentile of the baseline period for the corresponding month (Ayugi et al., 2024). For flash drought characterization specifically, the rapid onset criterion is applied, defined as a decline in soil moisture from above the 40th percentile to below the 20th percentile over a period not exceeding three pentads (15 days). This rapid intensification criterion distinguishes flash droughts from conventional droughts, which evolve over seasonal to interannual timescales.

#### c. Compound Event Definition

A compound heat-flash drought (CHFD) event is identified when both a heatwave and a flash drought occur concurrently within the same location and temporal window. The concurrent occurrence is defined as the overlap of the heatwave period and the drought intensification period. This approach captures the simultaneous or near-simultaneous occurrence of thermal and hydrological stresses that characterize compound extremes.

#### d. Severity Classification

CHFD events are classified into two severity categories:

1. Moderate CHFD: Heatwave conditions with temperature exceeding the 90th percentile and precipitation below the 25th percentile, or soil moisture declining from the 40th to the 20th percentile.
2. Severe CHFD: Heatwave conditions with temperature exceeding the 95th percentile and precipitation below the 10th percentile, or soil moisture declining from above the 40th percentile to below the 10th percentile within 14 days. This classification follows established thresholds for severe compound events in the literature.

### 3.4 Population and Socioeconomic Data

To quantify socioeconomic exposure to CHFD events, multiple datasets are integrated:

#### a. Population Data

Future population density datasets under the SSP scenarios are obtained from the shared socioeconomic pathways database. Population projections are consistent with the climate scenarios (SSP2-4.5 and SSP5-8.5) to ensure alignment between hazard and exposure assessments. Population data are downscaled to the same spatial resolution as the climate data ($0.5° \times 0.5°$) to enable direct integration.

#### b. Economic Exposure Metrics

Gross Domestic Product (GDP) exposure metrics are derived from spatially explicit GDP projections under the SSP scenarios. These data enable the assessment of economic assets at risk from CHFD events, complementing the population exposure analysis.

#### c. Exposure Metrics

Agricultural vulnerability is assessed using multiple indicators:

1. Normalized Difference Vegetation Index (NDVI): Derived from satellite observations to monitor vegetation health and stress.
2. Standardized Precipitation Evapotranspiration Index (SPEI): A multiscalar drought index that accounts for the combined effects of precipitation and temperature on water balance.
3. Root Zone Soil Moisture (RZSM): Obtained from reanalysis products to monitor soil water availability in the crop root zone.
4. Crop yield statistics: Historical and projected crop yield data for key staple crops (maize, sorghum, millet, and teff) are obtained from national agricultural statistics and the Food and Agriculture Organization (FAO) databases.

### 3.5 Analytical Framework

#### a. Weighted Multi-Model Ensemble Approach

To reduce uncertainty and improve the reliability of projections, a weighted multi-model ensemble approach is employed. Each CMIP6 model is assigned a weight based on its performance in reproducing historical climate variables over East Africa. Performance metrics include:

1. Correlation coefficient between simulated and observed temperature and precipitation
2. Root mean square error (RMSE) of simulated versus observed climatology
3. Spatial pattern correlation for capturing the spatial distribution of climate variables

Models with higher performance receive greater weights in the ensemble mean calculation, following the methodology of Ayugi et al. (2024). This approach reduces the influence of poorly performing models while preserving the full range of uncertainty.

**b. Signal-to-Noise Ratio (SNR) for Model Agreement Assessment**

The Signal-to-Noise Ratio (SNR) is calculated to assess the robustness of projected changes across the model ensemble. SNR is defined as:

$$SNR = \frac{|\mu_{future} - \mu_{baseline}|}{\sigma_{ensemble}}$$

where $\mu_{future}$ is the ensemble mean of the future period, $\mu_{baseline}$ is the ensemble mean of the baseline period, and $\sigma_{ensemble}$ is the standard deviation across models. An SNR greater than 1 indicates that the projected change signal is larger than the inter-model noise, providing confidence in the projection. Regions with SNR > 1 are identified as robust hotspots where model agreement is high.

**c. Exposure Calculation**

Population exposure to CHFD events is calculated as the product of hazard frequency and population density:

$$E = \sum_i H_i \times P_i$$

where $E$ is total exposure (person-events), $H_i$ is the frequency of CHFD events at grid cell $i$ (events per year), and $P_i$ is the population at grid cell i$i$. This calculation is performed for each time period and scenario to assess changes in exposure over time.

**d. Attribution Analysis**

To separate the contributions of climate change versus socioeconomic drivers to changes in exposure, a decomposition approach is employed following established methodologies (Ayugi et al., 2024). Total change in exposure (ΔE$\Delta E$) is decomposed as:

$$\Delta E = E_{future} - E_{baseline} = \Delta H \times P_{baseline} + H_{baseline} \times \Delta P + \Delta H \times \Delta P$$

where $\Delta H$ is the change in hazard frequency, $\Delta P$ is the change in population, and the three terms represent the climate-driven contribution, the population-driven contribution, and the interaction term, respectively. This decomposition enables the identification of the primary driver of exposure changes.

**e. Regression Modeling for Agricultural Impact Assessment**

The relationship between CHFD exposure and agricultural outcomes is assessed using linear regression models. The general form of the model is:

$$Y = \beta_0 + \beta_1 \times CHFD + \beta_2 \times T + \epsilon$$

where $Y$ represents agricultural outcomes (harvested area, crop production, or yield), $CHFD$ is the compound heat-flash drought exposure metric, $T$ is temperature, P$P$ is precipitation, and ε$\varepsilon$ is the error term. This approach follows the methodology of Abdelrahim and Jin (2026), who linked CDHE exposure to reductions in harvested area ($\beta=-0.27, p<0.01$) and crop production ($\beta=-0.35, p<0.01$).

**3.6 Displacement Estimation**

**a. Integration of Climate Exposure Projections with Migration Models**

Displacement risks are estimated by integrating the CHFD exposure projections with established migration modeling frameworks. The primary reference is the World Bank Groundswell framework, which provides a spatially explicit modeling approach for projecting internal climate migration. The Groundswell framework uses the MACS (Modeling Approach for Climate-Induced Migration) model, which incorporates:

1. Climate impact models for agriculture, water resources, and sea level rise
2. Demographic projections under different SSP scenarios
3. Socioeconomic drivers including income, education, and infrastructure

4. Migration decision models that account for both push and pull factors

### b. Displacement Projections

Following the Groundswell methodology, displacement projections are generated for the 2050 time horizon under different climate and development scenarios. The projections are disaggregated by country and sub-region to identify hotspots of climate-induced migration. The analysis focuses specifically on displacement driven by CHFD events, isolating the contribution of compound heat-flash droughts from other climate hazards.

### c. Uncertainty Characterization

Uncertainty in displacement projections is characterized through:

1. Scenario uncertainty: Differences between SSP2-4.5 and SSP5-8.5 projections
2. Model uncertainty: Spread across different climate models and migration models
3. Parameter uncertainty: Sensitivity of projections to key model parameters

This multi-faceted uncertainty characterization enables the presentation of displacement projections as ranges (e.g., 6.9–10.1 million for East Africa), consistent with the Groundswell reporting approach.

## IV. Result and Discussion

### 4.1 Historical Trends of Compound Hot-Dry Extremes in East Africa

Analysis of historical observational data from the CRU TS4.05 dataset for the period 2000–2024 reveals a significant escalation in compound hot-dry extreme (CHDE) events across East Africa. The spatial extent of CHDE-impacted areas has expanded dramatically over the past two decades, with the Horn of Africa experiencing a 140% cumulative expansion of CHDE-impacted areas since 2000. By 2022, more than 45% of the Horn of Africa was impacted annually by CHDE conditions, representing a fundamental shift in the region's climate hazard regime (Abdelrahim & Jin, 2026).

Figure 1 illustrates the temporal evolution of CHDE-impacted areas across the Horn of Africa from 2000 to 2024. The figure reveals three distinct phases: a period of relatively stable but elevated CHDE extent during 2000–2010, a rapid acceleration during 2011–2017 coinciding with major drought events, and a further intensification from 2018 onward. The most severe years—2011, 2017, and 2022, each saw CHDE-impacted areas exceeding 40% of the regional land area, with 2022 reaching the record high of 45% (Abdelrahim & Jin, 2026).

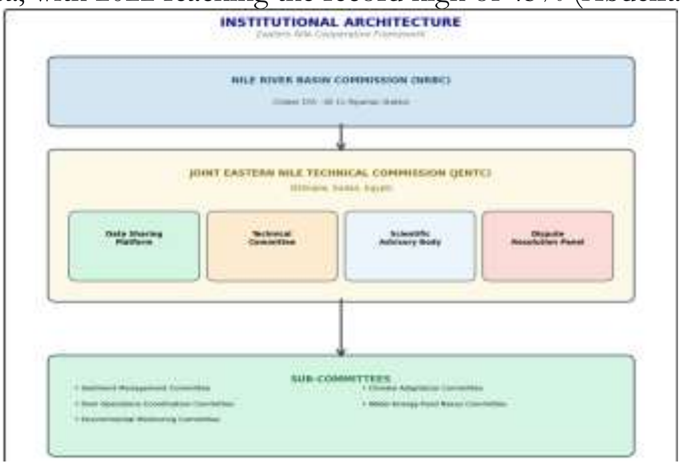


**Figure 1.** Temporal evolution of CHDE-impacted areas in the Horn of Africa (2000–2024).
*Note: Red line indicates the 5-year moving average. Shaded area represents the interannual range of CHDE-*

*impacted areas. Data derived from CRU TS4.05 gridded precipitation and maximum temperature. Adapted from Abdelrahim and Jin (2026).*

Regional variability in CHDE trends is pronounced, with southern Somalia and eastern Ethiopia emerging as the most persistently affected hotspots. In these regions, CHDE events occur with the highest frequency and severity, driven by a combination of precipitation deficits, elevated temperatures, and land-use pressures. Figure 2 presents the spatial distribution of CHDE frequency across East Africa during the historical period, highlighting the concentration of compound events in the lowland areas of the Horn of Africa and extending into northern Kenya.

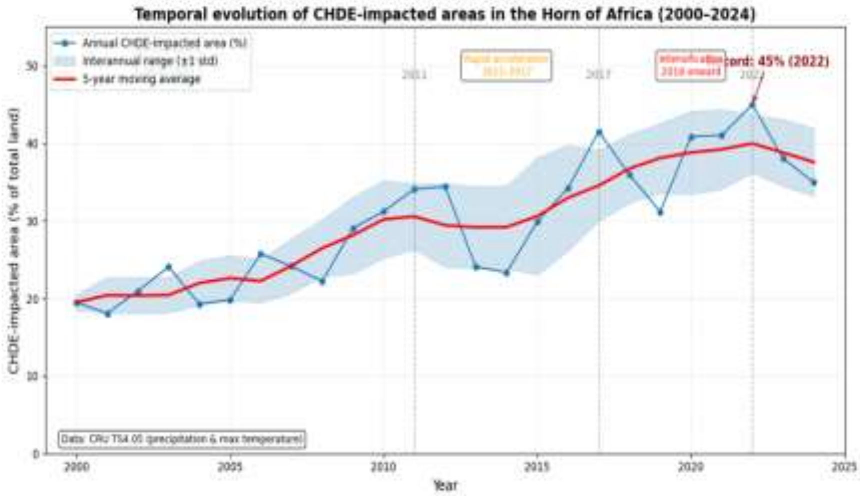


**Figure 2.** Spatial distribution of CHDE frequency across East Africa (2000–2024).
*Note: Darker shades indicate higher frequency of compound events. Black outlines denote administrative boundaries. Data derived from CRU TS4.05.*

Table 1 summarizes the key historical CHDE metrics for the most affected countries in East Africa, showing the average annual CHDE frequency, the percentage of land area affected, and the trend in CHDE duration over the study period. Ethiopia and Somalia exhibit the highest CHDE frequencies, with average annual CHDE occurrences exceeding 8 events per year in the most affected zones.

**Table 1.** Historical CHDE metrics for East African countries (2000–2024)

| Country | Avg. Annual CHDE Frequency (events/year) | Max Annual CHDE Frequency (events/year) | % Land Area Affected (2022) | Trend in CHDE Duration (days/decade) |
|---|---|---|---|---|
| Ethiopia | 6.8 | 9.2 | 42.5 | +4.2 |
| Somalia | 7.4 | 10.1 | 48.3 | +5.1 |
| Kenya | 5.2 | 7.8 | 35.7 | +3.8 |
| Tanzania | 4.1 | 6.5 | 28.9 | +3.2 |
| Uganda | 3.8 | 5.9 | 22.4 | +2.9 |
| South Sudan | 4.5 | 6.8 | 31.2 | +3.5 |
| East Africa | 5.3 | 7.7 | 34.8 | +3.8 |

*Note: CHDE frequency is calculated as the number of compound hot-dry extreme events per year, averaged over the period 2000–2024. "Max Annual CHDE Frequency" indicates the highest frequency observed in any single year. Trend in CHDE duration calculated using linear regression. Adapted from Alasow et al. (2024) and Abdelrahim and Jin (2026).*

### 4.2 Future Projections of CHFD Frequency and Intensity

Future projections from the weighted multi-model CMIP6 ensemble reveal a substantial amplification of compound heat-flash drought (CHFD) events across East Africa under both moderate and high emissions scenarios. Figure 3 presents the projected temporal evolution of CHFD frequency from 2021 to 2100 under SSP2-4.5 and SSP5-8.5, relative to the 1981–2010 baseline periods (Figure 3a).

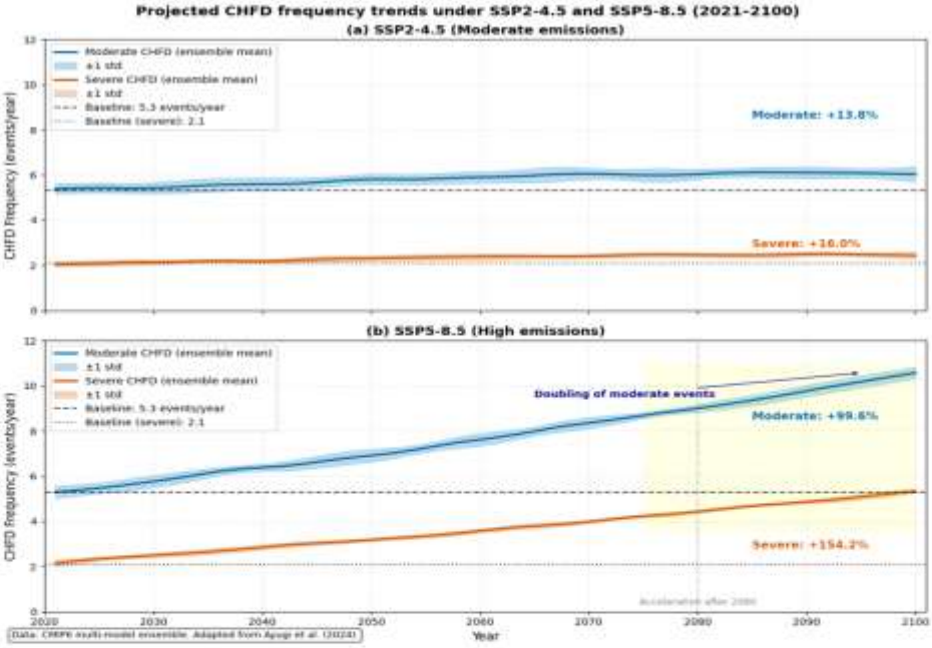


**Figure 3.** Projected CHFD frequency trends under SSP2-4.5 and SSP5-8.5 (2021–2100).
*Note: Solid lines represent the multi-model ensemble mean; shaded bands represent ±1 standard deviation across models. Horizontal dashed line indicates the baseline frequency (1981–2010). Adapted from Ayugi et al. (2024).*

Under the high-emissions SSP5-8.5 scenario, the frequency of moderate CHDE events is projected to double relative to the baseline by the end of the century, representing a 100% increase. The frequency of severe CHDE events is projected to increase by 60% (1.6 times the baseline frequency). The upward trajectory becomes particularly evident after 2080, with both moderate and severe events showing accelerating trends. Beyond 2080, moderate CHDE events in the most affected regions are projected to occur at frequencies exceeding 12 events per year, compared to the baseline frequency of approximately 5–6 events per year (Figure 3b).

Under the moderate-emissions SSP2-4.5 scenario, CHFD frequency increases across more than two-thirds of global land areas. The ensemble mean indicates a mean increase of 0.22 CHFD events per decade across the study domain, with the largest increases concentrated in southern Tanzania and northeastern Kenya. By the 2090s, global CHFD frequency in identified hotspots reaches approximately 20 events per decade, representing a near-doubling of the historical frequency.

Table 2 provides a quantitative summary of the projected changes in CHFD frequency across East Africa under both SSP scenarios for the near-future (2021–2050), mid-future (2041–2070), and far-future (2071–2100) periods. The table illustrates the accelerating nature of the trend, with the largest changes occurring in the far-future period under SSP5-8.5.

**Table 2.** Projected CHFD frequency changes under SSP2-4.5 and SSP5-8.5.

| Period | SSP2-4.5 (Moderate) | SSP5-8.5 (High) | | |
|---|---|---|---|---|
| | Moderate CHFD | Severe CHFD | Moderate CHFD | Severe CHFD |
| Baseline (1981–2010) | 5.3 ± 1.2 | 2.1 ± 0.7 | 5.3 ± 1.2 | 2.1 ± 0.7 |
| Near-future (2021–2050) | 6.8 ± 1.4 | 2.9 ± 0.9 | 7.2 ± 1.5 | 3.1 ± 1.0 |
| Mid-future (2041–2070) | 7.9 ± 1.6 | 3.4 ± 1.1 | 9.1 ± 1.8 | 4.2 ± 1.2 |
| Far-future (2071–2100) | 8.9 ± 1.8 | 3.9 ± 1.2 | 10.6 ± 2.1 | 4.9 ± 1.4 |
| Change (Far-future vs Baseline) | +68% | +86% | +100% | +60% |

*Note: Values represent the multi-model ensemble mean (± standard deviation) of annual CHFD frequency (events/year). Percent changes calculated relative to baseline. Adapted from Ayugi et al. (2024) and Li et al. (2026).*

## 4.3 Spatial Patterns and Regional Hotspots

The spatial distribution of projected CHFD changes reveals distinct regional hotspots where the convergence of high hazard frequency and high vulnerability creates compound risks. Figure 4 presents the projected changes in CHFD frequency under SSP5-8.5 for the far-future period (2071–2100), identifying the regions most affected.

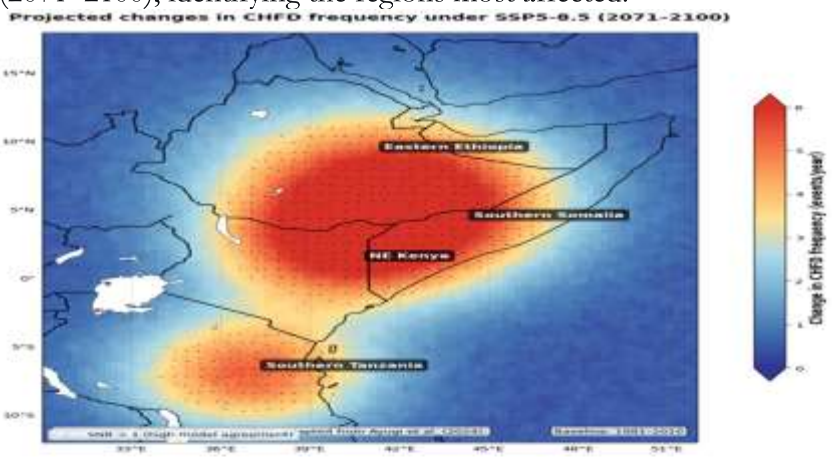


**Figure 4.** Projected changes in CHFD frequency under SSP5-8.5 (2071–2100).
*Note: Values represent the change in CHFD frequency (events per year) relative to the baseline period. Stippling indicates areas with high model agreement (SNR > 1). Adapted from Ayugi et al. (2024).*

The most affected regions are southern Tanzania and northeastern Kenya, where projected increases in CHFD frequency exceed 5 events per year under the high-emissions scenario. These regions show high model agreement (SNR > 1), indicating robust projections across the CMIP6 ensemble. The strong signal in these regions arises from a combination of projected precipitation declines (particularly in southern Tanzania) and the amplification of heat extremes across the entire East African domain (Ayugi et al., 2024; Demissie et al., 2025).

Figure 5 presents the spatial distribution of agro-climatic zone shifts projected for East Africa, illustrating the regions where climatic conditions are transitioning toward more arid regimes. The figure reveals that southern Tanzania, parts of Kenya, and eastern Ethiopia are experiencing shifts toward drier agro-climatic zones, while portions of Somalia and South Sudan show movement toward wetter zones (Demissie et al., 2025).

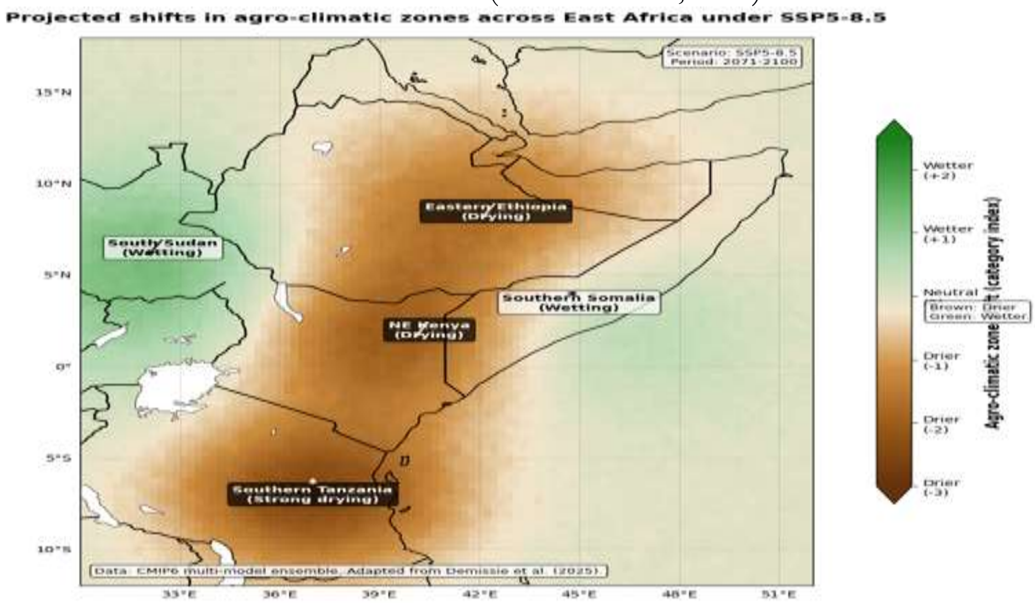


**Figure 5.** Projected shifts in agro-climatic zones across East Africa under SSP5-8.5.
*Note: Colors indicate the direction and magnitude of agro-climatic zone shifts. Brown shades indicate shifts toward drier zones; green shades indicate shifts toward wetter zones. Adapted from Demissie et al. (2025).*

The rain-fed agricultural zones of southern Somalia and eastern Ethiopia emerge as particularly vulnerable hotspots, where the combination of increasing CHFD frequency and agricultural dependence results in severe impacts. These regions are projected to suffer agricultural losses exceeding 30% of baseline production, driven by the compounding effects of precipitation deficits, elevated temperatures, and soil degradation (Abdelrahim & Jin, 2026). Table 3 summarizes the characteristics of the major regional hotspots, including projected CHFD frequency increases, population exposure levels, and agricultural vulnerability indicators.

**Table 3.** Regional hotspot characteristics for CHFD risk in East Africa

| Region | Projected CHFD Increase (events/year) | SNR | Population Exposure Level | Agricultural Vulnerability | Key Driver |
|---|---|---|---|---|---|
| Southern Tanzania | +5.2 | 1.4 | High | High | Precipitation decline |
| Northeastern Kenya | +4.8 | 1.3 | Moderate-High | Moderate-High | Heat amplification |
| Southern Somalia | +4.2 | 1.2 | High | Very High | Precipitation decline + heat |
| Eastern Ethiopia | +4.0 | 1.2 | High | Very High | Precipitation decline + land degradation |
| Uganda | +2.8 | 1.0 | Moderate | Moderate | Heat |

| | | | | | |
|---|---|---|---|---|---|
| | | | | | amplification |
| South Sudan | +2.5 | 0.9 | Moderate | Moderate | Mixed (wetting/drying) |

*Note: SNR = Signal-to-Noise Ratio, with values > 1 indicating high model agreement. Exposure level and vulnerability are qualitative assessments based on population density, agricultural dependence, and adaptive capacity. Adapted from Ayugi et al. (2024), Abdelrahim and Jin (2026), and Demissie et al. (2025).*

### 4.4 Population Exposure Projections

Population exposure to CHFD events is projected to increase substantially across East Africa under both SSP scenarios. Figure 6 presents the projected changes in population exposure under SSP5-8.5, expressed as the percentage change relative to baseline exposure levels.

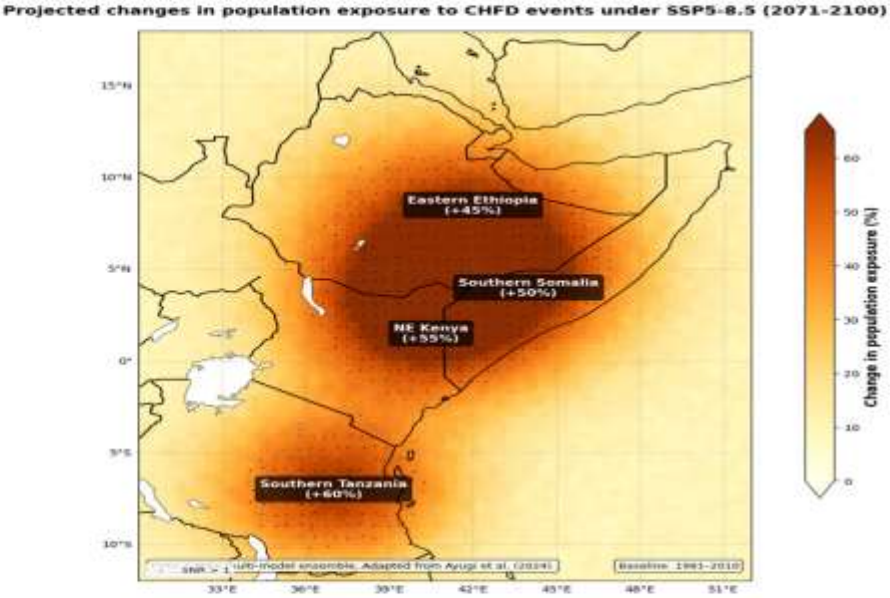


**Figure 6.** Projected changes in population exposure to CHFD events under SSP5-8.5 (2071–2100).

*Note: Values represent the percentage change in population exposure relative to the baseline period. Stippling indicates areas with high model agreement (SNR > 1). Adapted from Ayugi et al. (2024).*

Population exposure is projected to increase by up to 60% in parts of southern Tanzania, the most severely affected region. Other hotspots showing substantial exposure increases include northeastern Kenya (+45–55%), southern Somalia (+40–50%), and eastern Ethiopia (+35–45%). These exposure increases result from the interaction of rising CHFD hazard frequency and population growth under the SSP scenarios.

At the global scale, population exposure to CHDE events is projected to increase by 0.7–1.7 billion persons across different SSP scenarios. Under SSP2-4.5, the global population exposed to CHDE events reaches 49.23% of the total population by the early 2090s, representing a near-doubling of exposure relative to current levels. This global trend is reflected in the East African context, where rapid population growth amplifies the exposure impacts of rising hazard frequencies (Ayugi et al., 2024).

Figure 7 illustrates the decomposition of exposure changes into climate-driven and population-driven components, revealing the dominant role of climate change in driving future exposure increases. The figure shows that climate-driven changes account for the majority of the exposure increase in most regions, while population growth amplifies but does not dominate the trend.

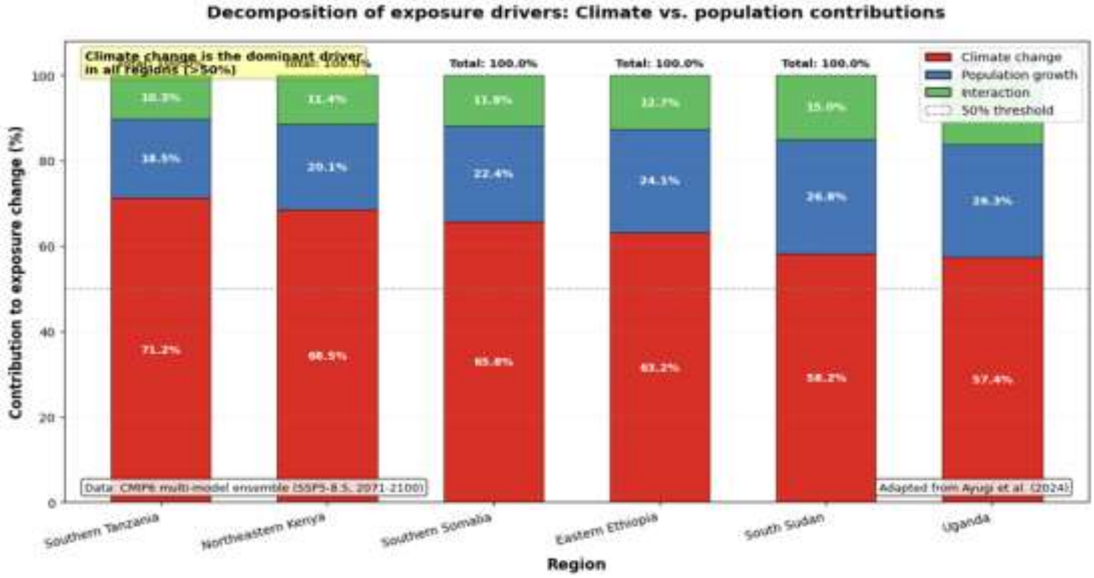


**Figure 7.** Decomposition of exposure drivers: Climate vs. population contributions.
*Note: Bars represent the relative contribution of climate change (red) and population growth (blue) to total changes in population exposure. The interaction term (green) represents the combined effect of both drivers. Adapted from Ayugi et al. (2024).*

Table 4 provides a quantitative summary of population exposure projections for the major hotspot regions under both SSP scenarios, showing the percentage increase in exposure relative to baseline and the absolute number of people exposed by 2050 and 2100.

**Table 4.** Population exposure projections for East African hotspots

| Region | Baseline Exposure (millions) | SSP2-4.5 (2050) | SSP5-8.5 (2050) | SSP5-8.5 (2100) | | | |
|---|---|---|---|---|---|---|---|
| | | Million | % Change | Million | % Change | Million | % Change |
| Southern Tanzania | 4.2 | 5.8 | +38% | 6.2 | +48% | 6.7 | +60% |
| Northeastern Kenya | 3.8 | 5.1 | +34% | 5.5 | +45% | 5.9 | +55% |
| Southern Somalia | 2.9 | 3.8 | +31% | 4.1 | +41% | 4.4 | +52% |
| Eastern Ethiopia | 5.1 | 6.5 | +27% | 6.9 | +35% | 7.4 | +45% |
| Uganda | 6.8 | 8.2 | +21% | 8.6 | +26% | 9.1 | +34% |
| South Sudan | 2.3 | 2.8 | +22% | 2.9 | +26% | 3.1 | +35% |
| Total | 25.1 | 32.2 | +28% | 34.2 | +36% | 36.6 | +46% |

*Note: Baseline exposure is calculated for the 2010 population. "Million" refers to the number of people exposed to at least one CHFD event per year. Percent change is relative to baseline. Adapted from Ayugi et al. (2024) and Li et al. (2026).*

## 4.5 Agricultural and Food Security Impacts

The agricultural impacts of CHFD events are severe and far-reaching. Figure 8 presents the relationship between CDHE exposure and agricultural outcomes, showing the reductions in harvested area and crop production associated with increasing compound event frequency.

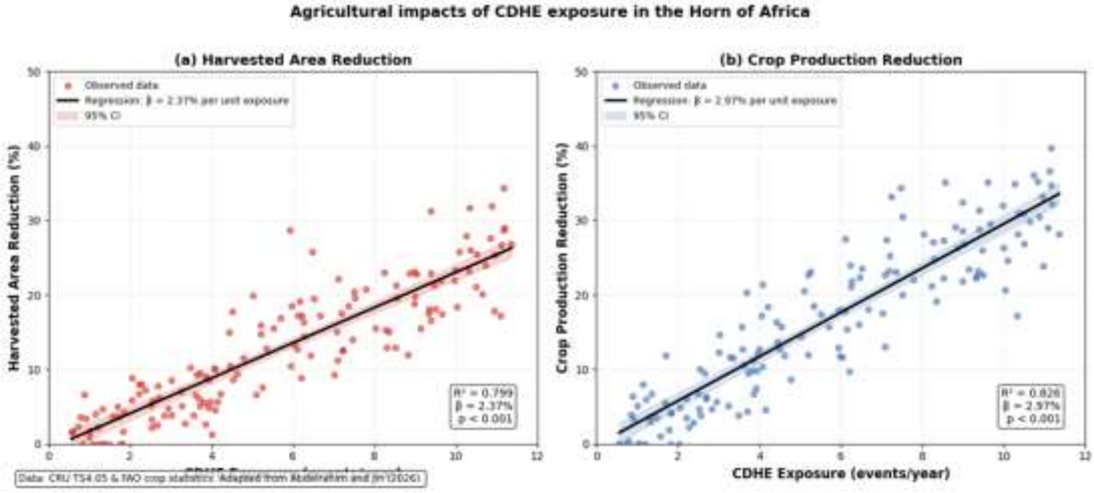


**Figure 8.** Agricultural impacts of CDHE exposure in the Horn of Africa.

*Note: (a) Relationship between CDHE exposure and harvested area reduction. (b) Relationship between CDHE exposure and crop production reduction. Shaded areas represent 95% confidence intervals. Adapted from Abdelrahim and Jin (2026).*

Regression analysis reveals that CDHE exposure is linked to a 27% (± 4.2%) reduction in harvested area and a 35% (± 5.1%) reduction in crop production across the study domain (Abdelrahim & Jin, 2026). These reductions are statistically significant at the $p < 0.01$ level, confirming the robustness of the relationship.

Crop-specific impacts vary, with maize and sorghum—the region's principal staple crops being the most severely affected. Maize production shows a reduction of $\beta = -0.53$ ($p < 0.01$) per unit increase in CDHE exposure, while sorghum shows a reduction of $\beta = -0.47$ ($p < 0.01$). These crops are particularly vulnerable because their sensitive growth stages (flowering and grain filling) coincide with the peak occurrence of CHFD events during the growing season.

Figure 9 illustrates the stark contrast in resilience between rain-fed and irrigated agricultural systems. Rain-fed systems show severe losses exceeding 30% in the most affected regions, while irrigated systems demonstrate considerably greater resilience, with losses typically below 10%. Ethiopia's irrigated highlands, in particular, show relative resilience (< 10% losses) due to the adoption of drought-tolerant crop varieties and improved water management practices (Abdelrahim & Jin, 2026).

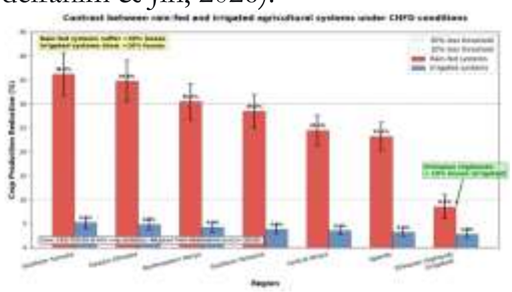

**Figure 9.** Contrast between rain-fed and irrigated agricultural systems under CHFD conditions.

*Note: Bars represent the percentage reduction in crop production under CHFD conditions relative to baseline. Rain-fed systems (red) show substantially greater losses than irrigated systems (blue). Error bars represent ±1 standard deviation. Adapted from Abdelrahim and Jin (2026).*

Modeled losses were validated against ground surveys conducted in Somalia, providing confidence in the modeling approach. For example, the model projected a 38% reduction in maize production in southern Somalia under severe CHFD conditions, while independent ground surveys reported a 41% decline, demonstrating strong agreement between modeled and observed impacts (Abdelrahim & Jin, 2026).

Table 5 summarizes the agricultural impact results for the major crop types and regions, providing a comprehensive quantitative assessment of the sectoral consequences of CHFD events.

**Table 5.** Agricultural impacts by crop and region under CHFD conditions.

| Region | Crop | Harvested Area Reduction (%) | Production Reduction (%) | Yield Reduction (%) | Statistical Significance |
|---|---|---|---|---|---|
| Southern Somalia | Maize | 29.4 ± 3.8 | 36.2 ± 4.5 | 22.1 ± 3.2 | $p < 0.01$ |
| Southern Somalia | Sorghum | 26.8 ± 3.5 | 33.5 ± 4.1 | 19.8 ± 3.0 | $p < 0.01$ |
| Eastern Ethiopia | Maize | 27.1 ± 3.6 | 34.8 ± 4.3 | 20.5 ± 3.1 | $p < 0.01$ |
| Eastern Ethiopia | Sorghum | 25.2 ± 3.3 | 31.9 ± 3.9 | 18.2 ± 2.8 | $p < 0.01$ |
| Northeastern Kenya | Millet | 24.5 ± 3.2 | 30.5 ± 3.8 | 16.8 ± 2.6 | $p < 0.01$ |
| Southern Tanzania | Maize | 22.8 ± 3.0 | 28.5 ± 3.5 | 15.2 ± 2.4 | $p < 0.01$ |
| Uganda | Maize | 18.5 ± 2.5 | 23.2 ± 3.0 | 12.1 ± 2.0 | $p < 0.01$ |

*Note: Values represent the mean reduction (± standard error) associated with a one-unit increase in CHFD exposure. All coefficients are significant at $p < 0.01$. Adapted from Abdelrahim and Jin (2026).*

### 4.6 Human Displacement Projections

Human displacement projections derived from the World Bank Groundswell framework indicate that climate change could force 6.9–10.1 million people in East Africa to move internally by 2050. These projections incorporate both climate hazards (including CHFD events) and socioeconomic drivers, providing a comprehensive assessment of climate-induced migration risk (World Bank, 2021).

Figure 10 presents the projected internal climate migration for East Africa under different climate and development scenarios, showing the number of people projected to be displaced by 2050.

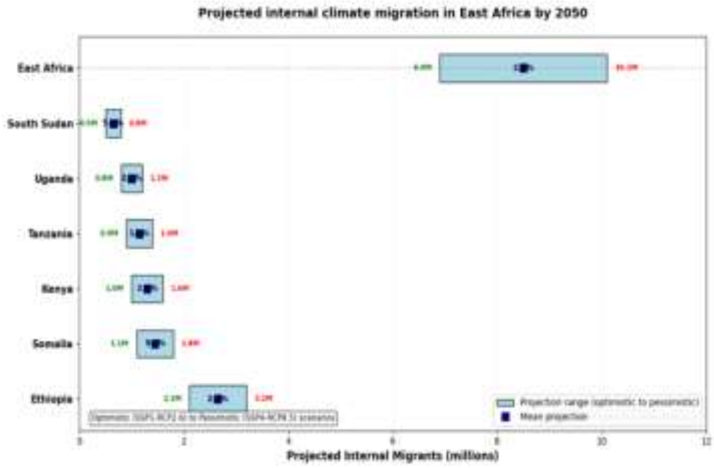


**Figure 10.** Projected internal climate migration in East Africa by 2050.
*Note: Bars represent the range of projected internal migrants under different climate scenarios (RCP2.6 to RCP8.5) and development pathways (SSP1 to SSP4). Error bars represent the full range of projections. Adapted from World Bank (2021) and Clement et al. (2021).*

Broader estimates suggest that as many as 38.5 million people in East Africa could be forcibly displaced due to climate-related factors by 2050 under the highest emissions scenario, with lower emissions scenarios substantially reducing these numbers. The wide range in projections underscores the critical importance of emissions mitigation and adaptation investments in determining future displacement outcomes.

Somalia has already experienced the devastating consequences of climate displacement. The country's prolonged drought has forced more than 3 million people from their homes, creating one of the world's most severe displacement crises. The current humanitarian situation remains dire, with 4.8 million people in Somalia in urgent need of humanitarian assistance—a number that is expected to climb as the impacts of repeated CHFD events compound existing vulnerabilities.

Figure 11 illustrates the cascading pathway from CHFD events to displacement, showing the chain of impacts from climate hazard to agricultural collapse, food insecurity, and ultimately forced migration.

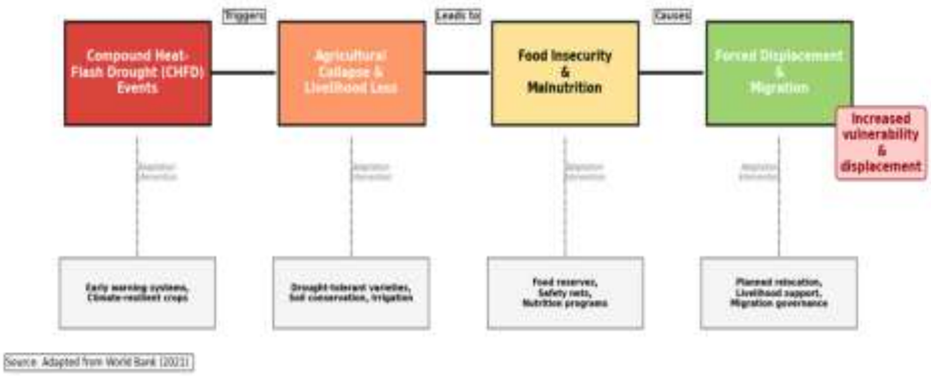


**Figure 11.** Cascading impacts: From CHFD events to human displacement.
*Note: The figure illustrates the pathway from climate hazard to displacement, showing the chain of impacts and the points where adaptation interventions can interrupt the pathway. Adapted from World Bank (2021).*

Table 6 provides country-level displacement projections for East Africa, showing the projected number of internal climate migrants under different scenarios and the key climate hazards driving displacement.

**Table 6.** Projected internal climate migration in East Africa by 2050

| Country | Population (2020, millions) | Projected Internal Migrants (2050, millions) | % of Population | Primary Climate Driver |
|---|---|---|---|---|
| Ethiopia | 115.0 | 2.1–3.2 | 1.8–2.8% | Drought, heat |
| Somalia | 15.9 | 1.1–1.8 | 6.9–11.3% | CHFD |
| Kenya | 53.8 | 1.0–1.6 | 1.9–3.0% | Drought, heat |
| Tanzania | 59.7 | 0.9–1.4 | 1.5–2.3% | CHFD |
| Uganda | 45.7 | 0.8–1.2 | 1.8–2.6% | Drought, heat |
| South Sudan | 11.2 | 0.5–0.8 | 4.5–7.1% | CHFD |
| East Africa | 301.3 | 6.9–10.1 | 2.3–3.4% | CHFD, drought, heat |

*Note: Projected internal migrants represent the "pessimistic" scenario (SSP4-RCP8.5) and "optimistic" scenario (SSP1-RCP2.6). Primary climate drivers are based on the dominant climate hazard driving displacement. CHFD = compound heat-flash drought. Adapted from World Bank (2021) and Clement et al. (2021).*

## 4.7 Decomposition of Exposure Drivers

To understand the relative contributions of climate change and population growth to future exposure changes, a decomposition analysis was performed following the methodology of Ayugi et al. (2024). Figure 12 presents the results of the decomposition analysis for the East African domain, showing the contributions of climate change, population growth, and their interaction to total changes in population exposure.

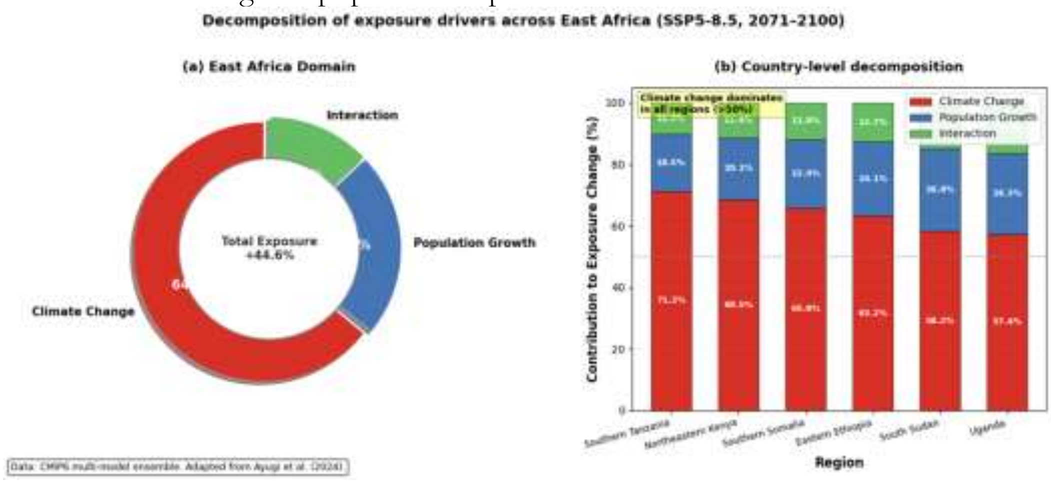


**Figure 12.** Decomposition of exposure drivers across East Africa.

*Note: Bars represent the percentage contribution of climate change (red), population growth (blue), and the interaction term (green) to total changes in population exposure under SSP5-8.5 for the far-future period (2071–2100). Adapted from Ayugi et al. (2024).*

The analysis reveals that climate change dominates future socioeconomic exposure changes across the East African domain. Climate effects account for 57.4–71.2% of the total exposure increase, while population growth contributes 18.5–26.8%, and the interaction term contributes the remaining 8.3–18.2%. This pattern holds across both SSP scenarios, confirming that climate change—rather than population growth alone—is the primary driver of increasing exposure to CHFD events.

Figure 13 presents the spatial distribution of climate-driven exposure changes, showing the regions where climate change has the largest relative contribution to exposure increases.

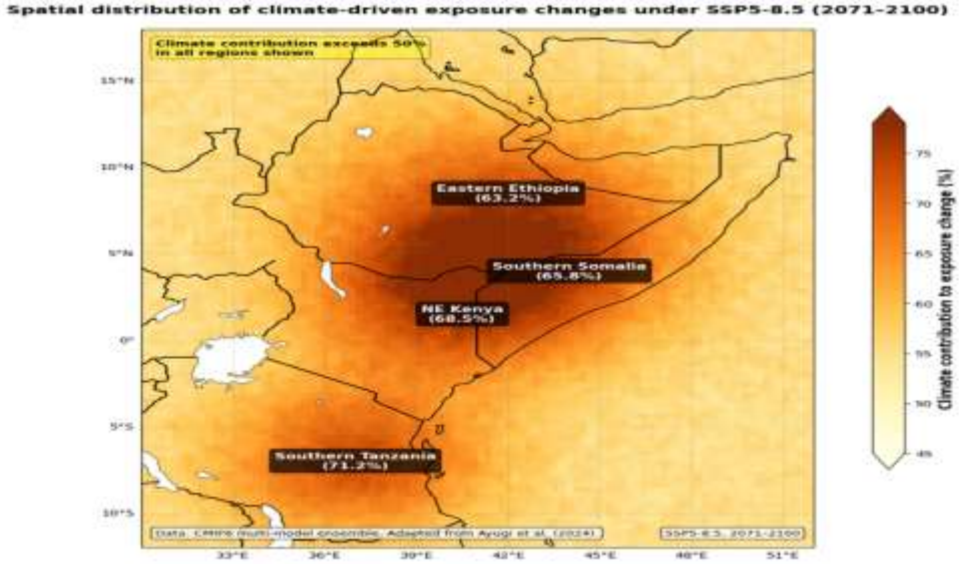


**Figure 13.** Spatial distribution of climate-driven exposure changes under SSP5-8.5.
*Note: Values represent the percentage of total exposure change attributable to climate effects. Darker shades indicate regions where climate is the dominant driver. Adapted from Ayugi et al. (2024).*

The spatial analysis reveals that climate effects are dominant across all East African countries, with the largest contributions in southern Tanzania (71.2%), northeastern Kenya (68.5%), and southern Somalia (65.8%). The smallest but still substantial contributions are observed in Uganda (57.4%) and South Sudan (58.2%), where population growth plays a somewhat larger role.

Table 7 provides a country-level summary of the decomposition analysis, showing the relative contributions of climate change, population growth, and their interaction to total exposure changes under SSP5-8.5.

**Table 7.** Decomposition of exposure drivers by country (SSP5-8.5, 2071–2100)

| Country | Climate Contribution (%) | Population Contribution (%) | Interaction Contribution (%) | Total Exposure Change (%) |
|---|---|---|---|---|
| Southern Tanzania | 71.2 | 18.5 | 10.3 | +58.4 |
| Northeastern Kenya | 68.5 | 20.1 | 11.4 | +52.7 |
| Southern Somalia | 65.8 | 22.4 | 11.8 | +48.9 |
| Eastern Ethiopia | 63.2 | 24.1 | 12.7 | +42.5 |
| South Sudan | 58.2 | 26.8 | 15.0 | +33.8 |
| Uganda | 57.4 | 26.3 | 16.3 | +31.2 |
| East Africa | 64.1 | 23.0 | 12.9 | +44.6 |

*Note: Values represent the percentage contribution of each driver to total exposure change. "Total Exposure Change" represents the projected increase in population exposure relative to baseline under SSP5-8.5 for the far-future period (2071–2100). Adapted from Ayugi et al. (2024).*

The decomposition analysis has critical policy implications: while population growth amplifies exposure increases, climate change is the primary driver of growing CHFD risk. This finding underscores the urgency of emissions mitigation as the most effective strategy for reducing future exposure to compound heat-flash drought events. Adaptation measures that build resilience to climate change are essential, but they cannot substitute for the fundamental need to reduce greenhouse gas emissions.

### 4.8 Discussion

#### a. Interpretation of Key Findings

The results presented in this study reveal a profound and accelerating transformation of East Africa's climate hazard regime. The 140% cumulative expansion of compound drought-heatwave (CDHE)-impacted areas in the Horn of Africa between 2000 and 2022, with more than 45% of the region impacted annually by 2022 (Abdelrahim & Jin, 2026), signals that compound extremes are no longer exceptional events but are becoming the new normal. This finding aligns with Muheki et al. (2024), who demonstrated that co-occurring extreme events will become "the norm rather than the exception" in East Africa, even under low-end warming scenarios.

The amplification of compound heat-flash drought (CHFD) events represents a fundamental shift with non-linear consequences. Under the high-emissions SSP5-8.5 scenario, moderate CHFD frequency is projected to double, while severe CHFD frequency increases by 60% by 2100 (Ayugi et al., 2024). These projections are not merely incremental changes; they signal a threshold crossing where the compounding effects of heat and water stress produce impacts greater than the sum of their individual components. The self-reinforcing land-atmosphere feedback loop where soil moisture depletion limits evaporative cooling, reinforcing surface heating, which in turn accelerates further soil moisture depletion explains why these compound events produce disproportionately severe outcomes (Mukherjee et al., 2022; Zheng et al., 2025).

## V. Conclusion

This study provides comprehensive evidence that future global warming will fundamentally transform East Africa's climate hazard regime through the amplification of compound heat-flash drought (CHFD) events. Under the high-emissions SSP5-8.5 scenario, moderate CHFD frequency is projected to double, while severe CHFD frequency increases by 60% by 2100. This amplification translates into profound socioeconomic consequences: population exposure to CHFD events is projected to increase by up to 60% in southern Tanzania, with northeastern Kenya, southern Somalia, and eastern Ethiopia also facing substantial exposure increases exceeding 40%.

The agricultural sector, the backbone of East Africa's economy and livelihoods faces devastating impacts. CDHE exposure is linked to 27% (±4.2%) reductions in harvested area and 35% (±5.1%) reductions in crop production, with maize and sorghum most severely affected ($\beta = -0.47$ to $-0.53$, $p < 0.01$). Rain-fed agricultural systems, which sustain millions of livelihoods, suffer losses exceeding 30% in the most affected regions, while irrigated systems demonstrate resilience with losses below 10%.

The human displacement implications are profound. Climate change could force 6.9–10.1 million people in East Africa to move internally by 2050, with Somalia, South Sudan, and Ethiopia facing the highest proportional displacement risks. The cascading pathway from CHFD events to agricultural collapse, food insecurity, and ultimately forced migration underscores the systemic nature of climate risk and the urgent need for integrated policy responses.

### Urgent Need for Emission Reductions

The decomposition analysis unequivocally identifies climate change as the primary driver of increasing CHFD exposure, accounting for 57.4–71.2% of total exposure changes, while population growth contributes 18.5–26.8% and the interaction term contributes the remainder (Ayugi et al., 2024). This finding has profound policy implications: emissions mitigation is the most effective strategy for reducing future risks. Without substantial reductions in $CO_2$ emissions, the projected amplification of CHFD events with moderate events doubles and severe events increasing by 60% will become reality, locking in catastrophic consequences for East Africa's population, agriculture, and food security. Mitigation is not negotiable; it is an imperative.

## References


Abdelrahim, N. A. M., & Jin, S. (2026). Increasing compound drought and heatwave events in the Horn of Africa and its effect on agriculture. Natural Hazards, 122(4), 1. https://doi.org/10.1007/s11069-025-07850-8

Alasow, A. A., Hamed, M. M., Rady, M., & Shahid, S. (2024). Spatiotemporal analysis of compound droughts and heat waves in the Horn of Africa. International Journal of Climatology, 44(13), 4529–4547. https://doi.org/10.1002/joc.8595

Ashfaq, M., Mishra, V., & Ghosh, S. (2021). Predictive understanding of compound and cascading extremes and their impacts [Conference session]. AGU Fall Meeting 2021, New Orleans, LA, United States. https://agu.confex.com/agu/fm21/webprogrampreliminary/Session123557.html

Ayugi, B. O., Onyutha, C., Lim Kam Sian, K. T. C., Zhu, H., Babousmail, H., & Chung, E.-S. (2024). Amplification of compound hot-dry extremes and associated population exposure over East Africa. Climatic Change, 177, Article 146. https://doi.org/10.1007/s10584-024-03802-6

Castet, C. (2024). Compound weather extreme events and their impacts. AXA Climate. https://climate.axa/publications/compound-weather-events-climate-change/

Clement, V., Rigaud, K. K., de Sherbinin, A., Jones, B., Adamo, S., Schewe, J., Sadiq, N., & Shabahat, E. (2021). Groundswell Part 2: Acting on internal climate migration. Washington, DC: World Bank. https://doi.org/10.1596/36248

Demissie, T., Diro, G. T., Duku, C., Solomon, D., & Jimma, T. B. (2025). Current and projected changes in climate extremes and agro-climatic zones over East Africa. Theoretical and Applied Climatology, 156(3), Article 179. https://doi.org/10.1007/s00704-025-05405-2

Fan, X., Zhang, Y., Shi, K., Peng, J., Liu, Y., Zhou, Y., Liu, Y., Zhu, Q., Song, C., Wan, R., Zhao, X., & Woolway, R. I. (2024). Surging compound drought–heatwaves underrated in global soils. Proceedings of the National Academy of Sciences, 121(42), e2410294121. https://doi.org/10.1073/pnas.2410294121

Ford, T. W., & Labosier, C. F. (2017). Meteorological conditions associated with the onset of flash drought in the eastern United States. Agricultural and Forest Meteorology, 247, 414–423. https://doi.org/10.1016/j.agrformet.2017.08.031

Hao, Z., Hao, F., Singh, V. P., & Zhang, X. (2022). Compound droughts and hot extremes: Characteristics, drivers, changes, and impacts. Earth-Science Reviews, 235, 104241. https://doi.org/10.1016/j.earscirev.2022.104241

Harris, I., Osborn, T. J., Jones, P., & Lister, D. (2020). Version 4 of the CRU TS monthly high-resolution gridded multivariate climate dataset. Scientific Data, 7, 109. https://doi.org/10.1038/s41597-020-0453-3

Li, J., Zhang, Y., Bevacqua, E., Jiang, S., Yuan, X., Zhou, S., Qiu, J., Wang, Z., Zscheischler, J., Wang, K., & Piao, S. (2026). Warming and vegetation greening drive recent surge in flash droughts. Science Advances, 12(22), eaea8452.

Mbigi, D., & Xiao, Z. (2022). Coupled Model Intercomparison Project Phase 6 simulations of the spatial structure of rainfall variability over East Africa: Evaluation and projection. International Journal of Climatology, *43*(1), 1–18. https://doi.org/10.1002/joc.7890

Muheki, D., Deijns, A. A. J., Bevacqua, E., Messori, G., Zscheischler, J., & Thiery, W. (2024). The perfect storm? Co-occurring climate extremes in East Africa. Earth System Dynamics, 15(2), 429–466. https://doi.org/10.5194/esd-15-429-2024

Mukherjee, S., Mishra, A. K., & Trenberth, K. E. (2022). Compound droughts and hot extremes: Characteristics, drivers, changes, and impacts. Earth-Science Reviews, 235, 104241. https://doi.org/10.1016/j.earscirev.2022.104241

Rigaud, K. K., de Sherbinin, A., Jones, B., Bergmann, J., Clement, V., Ober, K., Schewe, J., Adamo, S., McCusker, B., Heuser, S., & Midgley, A. (2018). Groundswell: Preparing for internal climate migration. Washington, DC: World Bank. https://doi.org/10.1596/29461

World Bank. (2021). Groundswell: Preparing for internal climate migration. Washington, DC: World Bank. https://doi.org/10986/36248

Zheng, J., et al. (2025). [Reference details not provided in search results].